

Electronic structure and magnetism in Ru-based perovskites

I. I. Mazin

*Complex Systems Theory Branch, Naval Research Laboratory, Washington, D.C. 20375-5320
and CSI, George Mason University, Fairfax, Virginia 22030*

D. J. Singh

Complex Systems Theory Branch, Naval Research Laboratory, Washington, D.C. 20375-5320

(Received 19 February 1997)

The magnetic properties of ruthenates with perovskite-derived structures, particularly $(\text{Ca,Sr})\text{RuO}_3$ and Sr_2YRuO_6 , are studied within the context of band-structure-based Stoner theory. First principles calculations are used to demonstrate that in all cases the correct magnetic behavior and order can be obtained without recourse to strong correlation effects and that the insulating character of Sr_2YRuO_6 is reproduced. The different magnetic states of SrRuO_3 and CaRuO_3 are shown to be due to the different structural distortions in these materials, most significantly the larger rotation of the octahedra in the Ca compound. CaRuO_3 is found to be on the verge of a ferromagnetic instability, leading to the expectation of giant local moments around magnetic impurities and other anomalous effects in analogy with fcc Pd metal. Oxygen $2p$ -derived states hybridize strongly with Ru d states in all three compounds, and O, through this hybridization, plays an unusually large role in the magnetic properties. This involvement of O is responsible for the strong magnetostructural coupling that is found in the calculations. Transport properties of CaRuO_3 and SrRuO_3 are analyzed using the calculated Fermiology. Unusually large magnon and paramagnon couplings are found, which are consistent with reported measurements of the low-temperature specific heat and the resistivity coefficient. [S0163-1829(97)05829-3]

I. INTRODUCTION

Mixed ruthenates with perovskite-based crystal structures have been receiving considerable attention of late,¹⁻²⁸ both because of their interesting magnetic properties and because of the recent discovery of superconductivity in the layered ruthenate Sr_2RuO_4 .¹⁶ Despite the rarity of $4d$ -based magnetic materials, SrRuO_3 is a robustly (Curie temperature $T_C \approx 165$ K, magnetization $m \approx 1.6\mu_B/\text{Ru}$) ferromagnetic metal occurring in a distorted cubic perovskite structure,²⁹⁻³³ and T_C can be even further increased by doping with Pb.¹³ However, magnetism is easily suppressed by doping with Ca, although Ca/Sr states are far removed from the Fermi level and accordingly may not be expected to influence the electronic properties of SrRuO_3 very drastically. Furthermore, Sr_2YRuO_6 , which has essentially the same crystal structure as SrRuO_3 , but with every second Ru substituted by Y, is antiferromagnetic, with estimates of the saturation magnetization even higher than the parent compound ($M \approx 3\mu_B$), although the critical temperature, T_N is reduced to 26 K. The variety of magnetic and electronic properties observed in these superficially similar compounds already poses an interesting theoretical challenge (cf., for instance, nonsuperconducting cuprates, which despite their large variety, always show strong antiferromagnetism in Cu-O planes). Besides, there are a number of interesting observations that deserve attention. These include the fact that SrRuO_3 is the only known ferromagnetic metal among the $4d$ oxides. As such interesting differences are expected from the much more abundant $3d$ oxide magnets. For example, much stronger spin-orbit effects compared to the $3d$ systems may be anticipated, and these may manifest themselves in the magnetocrystalline and magneto-optical properties. In fact,

SrRuO_3 does show an abnormally high magnetocrystalline anisotropy for a pseudocubic material³³ to the extent that it is difficult to measure its saturation magnetization using standard measurements of hysteresis loops, and resulting in some confusion in the older experimental literature. More recently, Klein and co-workers⁵ have measured strong magneto-optic properties in SrRuO_3 epitaxial films. $4d$ ions generally have more extended d orbitals than the corresponding $3d$ ions, and as a result $4d$ oxides tend to have greater overlap and hybridization between the transition metal and O $2p$ orbitals. Besides a tendency towards greater itinerancy, this can lead to more interplay between structural degrees of freedom and the magnetic and electronic properties.

As mentioned, additional interest in these ruthenates comes from their apparent proximity to superconductivity, and possible new insights into the problem of high-temperature superconductivity that may emerge from their study. Although the layered perovskite Sr_2RuO_4 has a modest T_c of 1 K (there have been very recent, unconfirmed reports of signatures of superconductivity at up to 60 K in the double perovskite Sr_2YRuO_6 with Cu doping³⁴), it was suggested that this material may be an unconventional superconductor. This is based largely on several similarities with the cuprates: Sr_2RuO_4 is isostructural with the first discovered high- T_c superconductor, shows highly two dimensional electronic properties, and of course is close to magnetic phases, particularly SrRuO_3 , and Sr_2YRuO_6 . However, the evidence for strong electron correlations in ruthenates is by far not yet as compelling as the body that has been accumulated for the cuprates and many other $3d$ oxides, and the question of whether these ruthenates can be treated within the framework of conventional band theory, or require a

strong-correlation based theory, remains open.

Several photoelectron spectroscopy experiments have been reported for Sr_2RuO_4 , which because of its layered crystal structure is more amenable to such studies than nearly cubic SrRuO_3 . Yokoya *et al.*²⁴ and Lu *et al.*,²⁵ using angle-resolved photoemission (ARPES), both report observation of Fermi surface sections and extended van Hove features somewhat like those in the local density electronic structure calculations, although the positioning of the van Hove singularity relative to the Fermi energy differs and the dispersion is generally somewhat weaker than in the calculations, probably due to correlations, but possibly because of strong electron-phonon and -magnon interactions. Similarly, Schmidt *et al.*²¹ observed the valence bands of Sr_2RuO_4 using ARPES, and found uppermost occupied bands with a width reduced by a factor of 2 compared with band structure calculations. Unfortunately, ARPES is highly sensitive to the quality of samples and particularly sample surfaces. Interestingly, polycrystalline but otherwise apparently high-quality Sr_2RuO_4 samples can be nonmetallic.³⁵ Angle-integrated photoemission is a more robust technique; using it, Yokoya *et al.*²³ found good agreement between the experiment and density functional calculations, but observe a correlation satellite to the d band (using resonant photoemission). Based on these measurements they estimated an effective Hubbard U of 1.5 eV, which is at least 3 times smaller than similar estimates for the cuprate superconductors, casting some doubt on suggestion that Sr_2RuO_4 and related ruthenates are very strongly correlated.

One of the most decisive arguments in favor of the importance of strong correlations in high- T_c cuprates is the failure of conventional local-density-approximation (LDA) band structure calculations to describe even qualitatively the antiferromagnetism in the undoped parent compounds. Similarly, the key question for these ruthenates may be which approximation, strongly correlated or band structure based, is best suited to explaining the variety of magnetic properties. One of the main purposes of this work is to determine whether a (similar to the cuprates) failure of the conventional, mean-field-type, band calculations is present in these ruthenates.

Within a strong-correlation scenario, the ferromagnetism in metallic SrRuO_3 , results from the double-exchange mechanism, while antiferromagnetism in insulating Sr_2YRuO_6 is due to superexchange via two (unlike the $3d$ oxides and Cu perovskites) oxygen ions. This is appealing because in the Mott-Hubbard picture the main factor controlling the magnetic properties is the carrier concentration, which is indeed different in those two materials: In $(\text{Sr,Ca})\text{RuO}_3$ ruthenium is four-valent, that is, its d band is populated by four electrons, while in Sr_2YRuO_6 the nominal valency of Ru is 5, and the number of d electrons is 3. On the other hand, integer occupancy does not favor the double-exchange scenario, and, besides, it is unclear how the Mott-Hubbard model provides a mechanism for suppressing magnetism in CaRuO_3 . Finally, as we discuss in detail below, conventional band theory in all the cases we test does yield the correct magnetic ground state, in contrast to the cuprates and similar correlated $3d$ -oxides. Thus, contrary to some recently suggested superconductivity scenarios based on strong correlations,^{26,36} it seems likely that if strong correlations

play some role, it is more of a quantitative than of a qualitative nature.

On the other hand, we note that even if Sr_2RuO_4 and other ruthenates are not strongly correlated, the superconductivity could still be unconventional, for instance, arising from a magnetic mechanism. In this regard, a number of measurements indicate anomalously large scattering of electrons by spin fluctuations,¹⁵ complicated by a strong magnetoelastic coupling.² Cyclotron masses,²² the specific heat, and the paramagnetic susceptibility¹⁶ are all strongly renormalized. While there is always the possibility of ascribing this renormalization to strong correlations, the simplest explanation may be strong electron-phonon-magnon interactions. Further, an abnormally large transport coupling constant λ_{tr} is required to rationalize the temperature dependence of the resistivity with the calculated Drude plasma energies,¹⁸ although this value is consistent with the specific heat enhancement. Unusual temperature dependences of the Hall effect²⁰ were found in CaRuO_3 and in SrRuO_3 . We shall return to the transport properties later in the paper; it is plausible that they can be reconciled with the conventional one-electron mechanism, despite the unusual T dependences.

The main purpose of the present paper is to study the magnetic phases and the relative importance of correlation and band structure effects for obtaining the magnetic properties. We focus on the double perovskite Sr_2YRuO_6 and the ferromagnetic-paramagnetic transition in $(\text{Sr,Ca})\text{RuO}_3$ with increasing Ca content, and we shall show that conventional band theory is fully able to describe the variegated magnetic properties in this family of materials.

II. FIRST PRINCIPLES CALCULATIONS

A. Structure, magnetism, and ionic considerations

As mentioned, SrRuO_3 occurs in an orthorhombic, $Pbnm$, GdFeO_3 structure, which has four formula units per cell. It is interesting to note that this is the same generic structure as LaMnO_3 and related manganites that have received considerable recent attention because of the discovery of colossal magnetoresistance effects in some of these. Further SrRuO_3 has the same nominal d electron count as LaMnO_3 , although unlike LaMnO_3 it is a ferromagnetic metal even without doping. In LaMnO_3 the distortion from the ideal cubic perovskite crystal structure consists of both rotations of the O octahedra and Jahn-Teller distortions of them to yield Mn-O bond length variations of more than 10%. This is understood in ionic terms as a result of the fact that the high-spin Mn ion with this electron count has a half-full majority spin e_g orbital favoring a Jahn-Teller distortion. In contrast, SrRuO_3 occurs with a reduced magnetic moment and its distortion consists of almost rigid rotations of the O octahedra with practically no accompanying variations in the Ru-O bond lengths.

CaRuO_3 occurs in the same crystal structure and symmetry as SrRuO_3 , also with no evident Jahn-Teller distortion of the O octahedra, but with approximately twice larger rotations. Such rotations are common in perovskite-based materials and are usually understandable in terms of ionic size mismatches between the A and B site cations. Such an explanation is consistent with the trend observed in $(\text{Sr,Ca})\text{RuO}_3$ since the Ca^{2+} ionic radius is approximately

0.15 Å smaller than Sr^{2+} . Although CaRuO_3 is paramagnetic, it is believed to be rather close to magnetic instability.

Sr_2YRuO_6 is an antiferromagnetic insulator that occurs in a distorted but well-ordered double-perovskite structure. This is derived from the perovskite SrRuO_3 by replacing every second Ru by Y, such that the remaining Ru ions form an fcc lattice. The structural units are thus Ru-O and Y-O octahedra, with the Sr ions in the A site positions providing charge balance. Each Ru-O octahedra shares a single O atom with each neighboring Y-O octahedra, and vice versa, but there are no common O ions shared between different Ru-O octahedra. The primary distortions from the ideal perovskite-derived structure consist of (1) a substantial breathing of the octahedra to increase the Y-O distance to 2.2 Å at the expense of the Ru-O distances which become 1.95 Å and (2) rotations of the octahedra to reduce the closest Sr-O distances, consistent with the ionic sizes. These distortions reduce the symmetry to monoclinic ($P21/n$). A related view of the crystal structure is based on the fact that Y, like Sr, is fully ionized in such oxides, and accordingly is a spectator ion providing space filling and charge to the active Ru-O system but playing no direct role in the electronic or magnetic properties. From this point of view, Sr_2YRuO_6 consists of independent rigid, but tilted, $(\text{RuO}_6)^{7-}$ octahedral clusters, arranged on a slightly distorted fcc lattice. Hopping then proceeds between Ru ions in neighboring RuO_6 clusters via two intervening O ions

Since Y is trivalent, the Ru is formally five-valent ($4d^3$) in this compound instead of formally tetravalent as in perovskite SrRuO_3 . In the octahedral crystal field, the Ru t_{2g} orbitals lie below the e_g orbitals, so that in the high-spin state the majority spin Ru t_{2g} manifold would be fully occupied, and all other Ru $4d$ orbitals unoccupied. This Jahn-Teller stable configuration is consistent with the experimental observation that the bond angles and bond lengths within the Ru-O octahedra are almost perfectly equal, but the Ru moment of $1.85\mu_B/\text{Ru}$ measured using neutron diffraction is considerably smaller than the $3\mu_B/\text{Ru}$ that would be expected in the high-spin configuration.

First principles studies of SrRuO_3 have shown that its electronic structure involves rather strong Ru-O covalency, and that O p -derived states participate substantially in the magnetism and the electronic structure near the Fermi energy, which is important for understanding the transport properties. As will be discussed below, a similar covalency is present in CaRuO_3 and the differences in the magnetic ground states of CaRuO_3 and SrRuO_3 are due to band structure effects related to the modulation of the Ru-O hybridization by the structural distortion. In this regard, it should be noted that Ru $^{5+}$ -O hybridization may be even stronger in Sr_2YRuO_6 , based on the expectation that the O $2p$ manifold would be even higher in energy with respect to the Ru d states. The similar Ru-O distances in SrRuO_3 and Sr_2YRuO_6 (less than 0.03 Å longer than in Sr_2YRuO_6) and the fact that 5 is not a common oxidation state for Ru also suggest strong covalency in the double perovskite. Here we report density functional calculations of the electronic and magnetic properties of Sr_2YRuO_6 . These confirm the strongly hybridized view of these materials and provide an explanation for the electronic and magnetic properties.

B. SrRuO_3

The electronic structure of SrRuO_3 has been described elsewhere.^{6,27} Here we repeat, for completeness, the main results, and also discuss some quantitative differences between the published calculations.

There have been two recent band structure calculations for SrRuO_3 .^{6,27} In both works the calculations were performed for both an idealized cubic perovskite structure and the experimental crystal structure. Allen *et al.*²⁷ interpreted their experimental measurements in terms of the band structure calculated within the local spin density approximation (LSDA) using the linear muffin-tin orbital (LMTO) method. Singh⁶ used the general potential linearized augmented plane-wave (LAPW) method to calculate electronic and magnetic properties. The two studies yielded reasonably similar results for the electronic structures near the Fermi energy although some noticeable differences are present. Important for interpreting experimental results are the differences in the density of states and in the Fermi velocities. The latter were found in Ref. 6 to be almost isotropic, while in Ref. 27 strong anisotropy of the Fermi velocity (about 30% in each channel) was reported. The ratio N_\uparrow/N_\downarrow found in Ref. 27 is 50% larger than that in Ref. 6. Most important, the overall shape of the density of states within a ± 0.2 Ry window at the Fermi level is rather different. It is known that the accuracy of the atomic sphere approximation calculations can be difficult to control for materials with open crystal structures and low site symmetries due to sensitivity to the computational parameters (e.g., basis set, inclusion of empty spheres in lattice voids, linearization parameters, etc.). Since we wanted to use LMTO atomic-sphere-approximation (ASA) technique in analyzing the calculated band structure, we have repeated the LAPW calculations reported in Ref. 6 using a standard LMTO-ASA package STUTTGART-4.7. We found it necessary to include ten empty spheres per formula unit to achieve adequate space filling in the distorted structure (in the cubic perovskite structure this was not needed). The result appeared to be much closer to the LAPW results of Ref. 6 than to the LMTO ones of Ref. 27; Ref. 27 does not mention use of any empty spheres, in which case insufficient space filling could have influenced the calculation. The results given here are from LAPW calculations, except where specifically noted otherwise.

Calculations for SrRuO_3 in the ideal perovskite structure yielded a spin moment of $1.17\mu_B$ per formula unit, while calculations including the experimentally observed rotations yielded a larger moment of $1.59\mu_B$ in accordance with recent experimental results. Only a portion of the total moment resides on the Ru sites (64% in the LAPW MT sphere, and 67% in the LMTO atomic sphere). The electronic density of states has a gap in the spin majority channel which is only 20 mRy above the Fermi level. The fact that SrRuO_3 is so close to a half-metal is important for understanding its transport properties, and the fact that they are so sensitive to magnetic ordering (and, correspondingly, to temperature).

C. CaRuO_3

Experimentally, CaRuO_3 is a paramagnetic metal. This fact suggests that the rotation of the RuO_6 octahedra is antagonistic to magnetism (since larger rotations constitute the

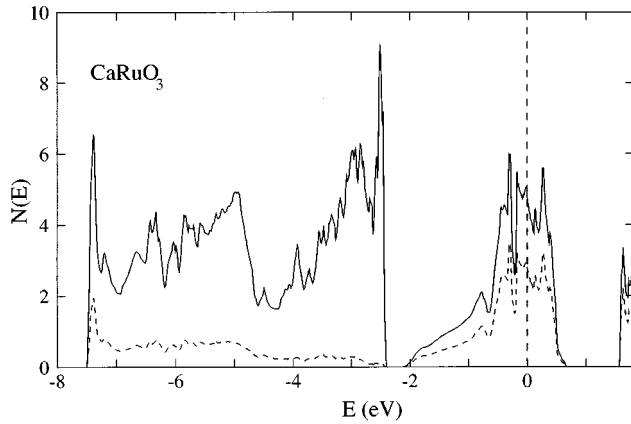


FIG. 1. LAPW density of states of CaRuO_3 in its actual crystal structure. The total density of states is shown by the solid line. Only Ru (d) partial density of states is shown (dashed line), because the O (p) density is approximately the difference between the total and the Ru (d) densities. Here and in the other figures all densities of states are per spin and formula unit.

main structural difference between CaRuO_3 and SrRuO_3). However, this conjecture is apparently at odds with the calculated result that the equilibrium magnetization in SrRuO_3 is smaller in an ideal cubic perovskite structure than in the actual distorted one. As a first step to understanding this, we have extended our calculations to CaRuO_3 in its experimental structure. Details of the method are as in Ref. 6. The resulting density of states is shown in Fig. 1. We find that indeed the magnetism is suppressed in this case, though in a very borderline fashion. Fixed spin moment calculations of the total energy as a function of spin magnetization for CaRuO_3 show a very extended flat region, extending to near $1.5\mu_B$ per formula unit. This is reminiscent of fcc Pd which also shows such a flat region. This borderline state implies a high-spin susceptibility and explains the fact that low doping can induce a ferromagnetic state. Further, paramagnon-like spin excitations should be very soft in this material and magnetic impurities may be expected to induce giant induced local moments. There are already some reports that this is the case in CaRuO_3 .³⁷

Having shown that the ferromagnetism in SrRuO_3 and its suppression in CaRuO_3 can be described using band structure methods, we turn to the question of why these two perovskites have different magnetic properties. To determine whether the key difference between the materials is structural we have performed calculations for CaRuO_3 using the crystal structure of SrRuO_3 . These calculations yield a spin magnetization of $1.68\mu_B$ per formula unit and a magnetic energy of 0.06 eV/Ru, very similar to SrRuO_3 . Calculations for the intermediate structure formed by a linear average of the experimental CaRuO_3 and SrRuO_3 structures yield a similar spin moment of $1.53\mu_B$ per formula unit and a magnetic energy of only 0.029 eV/Ru (note the similarity of the magnetizations and large variation of magnetic energy). To within the accuracy of our calculations this paramagnetic-ferromagnetic energy difference becomes zero just at the experimental CaRuO_3 structure. Since ferromagnetism in the $(\text{Sr,Ca})\text{RuO}_3$ is apparently strongly coupled to the rotation of the octahedra, alloying the A site cation is expected to be an effective means for tuning the magnetic properties. Alloying

CaRuO_3 with larger divalent cations should generally induce ferromagnetism while alloying SrRuO_3 with smaller cations should suppress ferromagnetism. BaRuO_3 , while a known compound, occurs in a different crystal structure and is not magnetic. However, Pb can be partially substituted on the Sr site, and it is known that introduction of this slightly larger divalent cation does increase T_C in SrRuO_3 .

Later in the paper we shall analyze the transformation of the band structure of $(\text{Sr,Ca})\text{RuO}_3$ upon increase of the tilting in more detail and will show that the nonmonotonic dependence of the equilibrium magnetization on tilting is a straightforward consequence of a natural evolution of the band structure near E_F with the structural distortion.

D. Sr_2YRuO_6

The electronic and magnetic structure of Sr_2YRuO_6 was calculated using the full experimental crystal structure of Battle and Macklin³⁸ except that the very small (0.23%) lattice strain was neglected. Additional calculations were performed for idealized structures neglecting the tilting of the octahedra to help understand the role of this distortion, which changes the angles and distances along the Ru-O-O-Ru hopping paths. These local-density-approximation calculations were performed using the general potential LAPW method³⁹ including local orbital extensions⁴⁰ to accurately treat the O $2s$ states and upper core states of Sr and Y as well as to relax any residual linearization errors associated with the Ru d states. A well-converged basis consisting of approximately 2700 LAPW basis functions in addition to the local orbitals was used with O sphere radii of 1.58 a.u. and cation radii of 2.10 a.u. This self-consistent approach has a flexible representation of the wave functions in both the interstitial and sphere regions and makes no shape approximations to either the potential or charge density. As such it is well suited to materials with open structures and low site symmetries like Sr_2YRuO_6 . In addition, we used the LMTO method in the atomic sphere approximation and tight-binding representation⁴¹ (STUTT-GART-4.7) to get better insight in the calculated electronic structure. The LMTO-ASA method is less accurate than the full-potential LAPW but it provides more flexibility in the way how the results are represented and how they can be analyzed in tight-binding language.

Calculations were performed at the experimental structure for ferromagnetic (F) and the observed antiferromagnetic (AF) orderings. The AF ordering is 0.095 eV/Ru lower in energy than the F ordering, and has an insulating gap in the band structure, consistent with the experimental ground state. The insulating gap of 0.08 eV is between majority and minority spin states and may yield only a weak optical signature. The Ru moment as measured by the magnetization within the Ru LAPW sphere is $1.70\mu_B$ for the AF state and $1.80\mu_B$ with the F ordering, in reasonable accordance with the neutron scattering results. The similar moments with different spin configurations suggest that a local moment picture of the magnetism is appropriate for Sr_2YRuO_6 . This is in contrast to perovskite SrRuO_3 . Similar to SrRuO_3 there are substantial moments within the O LAPW spheres as well as the Ru spheres, amounting to approximately $0.10\mu_B/\text{O}$ (AF ordered) and $0.12\mu_B/\text{O}$ (F ordered). These cannot be understood as tails of Ru $4d$ orbitals extending beyond the

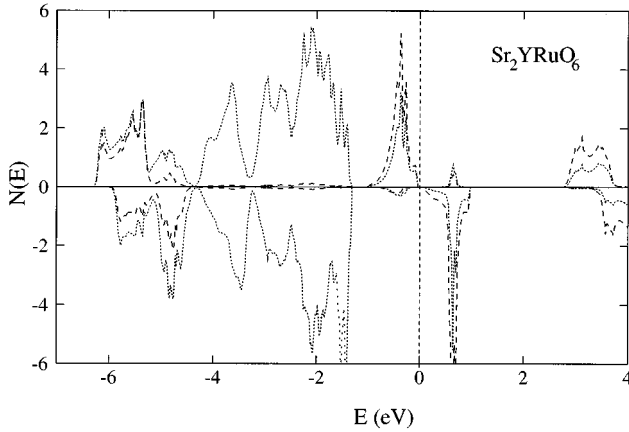


FIG. 2. LAPW density of states of antiferromagnetic Sr_2YRuO_6 . Partial densities of states of Ru (d) and O (p) orbitals are shown by the dashed and dotted lines, respectively.

LAPW sphere radii, since such an explanation is inconsistent with the radial dependence of these orbitals, but rather they arise from polarization of the O ions due to hybridization, which is evidently strong both from this point of view and from the calculated electronic structure, discussed below. The total local moment per formula unit is of mixed Ru and O character and amounts to $3\mu_B/\text{f.u.}$, which is approximately 60% Ru derived and 40% O derived [the interstitial polarization of $(0.5-0.7)\mu_B/\text{cluster}$ derives from both Ru and O, but is assigned as mostly O in character based on the extended $2p$ orbitals of negative O ions and the small O sphere radius, and results of LMTO-ASA calculations, which do not have any interstitial volume]. The calculated exchange splittings of the O $1s$ core levels are 80 to 95 meV depending on the particular O site. The O polarizations may be observable in neutron experiments if O form factors are included with Ru in the refinement. Such an experiment is strongly suggested by the present results.

Projections of the electronic density of states (DOS) of antiferromagnetic Sr_2YRuO_6 onto the LAPW spheres are shown in Fig. 2, where majority and minority spin projections onto a Ru ion and the six O ions in its cluster are shown. The DOS in two spin channels are similar in shape apart from an exchange splitting throughout the valence energy region and show evidence of a strongly hybridized electronic structure. The details of this structure are deferred to the tight-binding (TB) analysis below, except to mention the exchange splitting of the essentially pure O $2p$ states between -4 and -6 eV relative to the Fermi energy (E_F) and the fact that there are substantial Ru $4d$ contributions to the minority spin channel between -4 and -6 eV as well as O contributions above E_F , implying that the average Ru $4d$ occupancy is considerably higher than d^3 . Although assigning charge in a crystal to various atoms is an ambiguous procedure, integration of the d -like DOS implies an average near d^5 similar to perovskite SrRuO_3 . The magnetic moments derive from polarization of three bands near E_F by an exchange splitting of 1 eV. The F -ordered DOS (Fig. 3) is very similar to that in the AF state, but the exchange splitting is somewhat smaller and the bandwidth somewhat larger, resulting in a slight semimetallic overlap of majority and

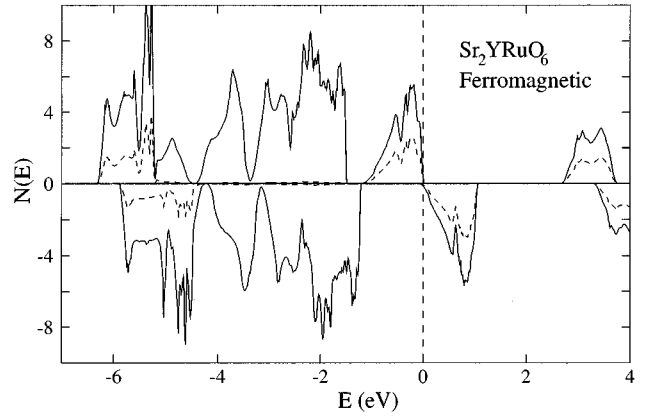


FIG. 3. LAPW density of states of ferromagnetic Sr_2YRuO_6 . Partial density of states of Ru (d) orbitals and the total density of states are shown by the dashed and solid lines, respectively.

minority spin bands at E_F which reduces the spin moment from $3.0\mu_B/\text{f.u.}$ to $2.97\mu_B/\text{f.u.}$

Parallel calculations were performed using a structure in which the tilting of the RuO_6 clusters is suppressed. As with the actual experimental structure, the AF ordering is lower in energy than the F ordering. However, in this case the band structures are metallic for both orderings, showing that the tilting is crucial for the insulating state. As will be discussed below there is a substantial coupling between the magnetic order and this structural degree of freedom.

III. TIGHT-BINDING INTERPRETATION AND PHYSICAL PROPERTIES

A. Sr_2YRuO_6

1. Single RuO_6 cluster

Somewhat unexpectedly, the easiest compound to understand is the Sr_2YRuO_6 double perovskite. Sr and Y, as is common in perovskites, are fully ionic, so that the states around the Fermi level barely have any Sr or Y character. Thus, as mentioned, this compound can be viewed as consisting of rigid RuO_6 octahedra, arranged on a fcc lattice, and loosely connected to each other. We will show below that this intuitive picture provides very good qualitative and quantitative interpretation of the full-scale band structure calculation. In contrast with Sr_2RuO_4 or $\text{Sr}_x\text{Ca}_{1-x}\text{RuO}_3$, no octahedra share oxygens. The octahedra are slightly tilted, which we shall neglect for the moment (the effect of tilting is in a certain sense important and will be discussed later). Accordingly, we begin by discussing a single cluster.

The electronic structure of a single RuO_6 cluster is governed by the relative position of Ru d and O p levels, and the corresponding hopping amplitudes. The Ru d states are split by the crystal field into two manifolds consisting of three t_{2g} and two e_g levels, respectively, and these are separated by ≈ 1 eV. The O p levels are subject to a crystal field splitting at least three times smaller, and yield 9 p_π states, which form $pd\pi$ bonds with Ru, plus three p_σ states, which participate in the $pd\sigma$ bonding. After including pd hopping, the system of levels becomes, for each spin channel: 13 non-bonding, $4 \times E_0(p_\sigma) + 9 \times E_0(p_\pi)$; 5 bonding, $2 \times E_-(E_g) + 3 \times E_-(T_{2g})$; and 5 antibonding, $2 \times E_+(E_g) + 3$

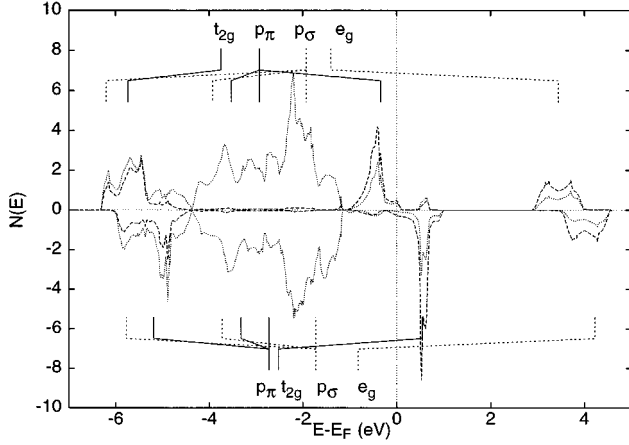


FIG. 4. Calculated LAPW density of states for cubic Sr_2YRuO_6 (antiferromagnetic) and the level scheme for an individual RuO_6 cluster. Notation for the density of states is the same as in Fig. 2. T_{2g} levels and their parent states are shown by solid lines, the E_g levels and states by dashed lines. Compared with the formulas in Sec. III A 1, additional small O-O hoppings τ_π and τ_σ are taken into account; these split off the nonbonding levels mixed oxygen states with $E_0(p_\sigma) - 4\tau_\sigma$ and $E_0(p_\pi) - 2\tau_\pi$.

$\times E_+(T_{2g})$, where E_0 are pure ionic levels, and

$$E_\pm(E_g) = 0.5\{E_0(p_\sigma) + E_0(e_g) \pm \sqrt{[E_0(p_\sigma) - E_0(e_g)]^2 + 16t_\sigma^2}\},$$

$$E_\pm(T_{2g}) = 0.5\{E_0(p_\pi) + E_0(t_{2g}) \pm \sqrt{[E_0(p_\pi) - E_0(t_{2g})]^2 + 16t_\pi^2}\}.$$

The actual ordering of levels in RuO_6 , as shown on Fig. 4, is $E_-(T_{2g}) \approx E_-(E_g) < E_0(p_\sigma) < E_0(p_\pi) < E_+(T_{2g}) \ll E_+(E_g)$. The last inequality leads to a substantial gap (> 2 eV) between the antibonding T_{2g} and the antibonding E_g bands in the solid. This large gap is only partially due to the crystal field, and arises largely from the stronger (relative to $pd\pi$) $pd\sigma$ bonding. The exchange splitting is, naturally, weaker than this enhanced crystal field splitting, and the Hund's rule does not apply to the high-lying antibonding E_g states, which remain empty in both spin channels. Neglecting those states, there are 21 levels to be occupied by 39 valence electrons. Here Hund's rule does apply and tells us to populate all 21 spin-majority states, and all but the three antibonding T_{2g} levels in the spin-minority channel. Thus for the electronic properties of the crystal these six spin-up and spin-down T_{2g} molecular orbitals are of primary relevance; the symmetry of these orbitals is the same as for $d(t_{2g})$ states in a transition metal ion. We now use this information to analyze the electronic structure of crystalline Sr_2YRuO_6 .

2. Intercluster hopping and exchange

When a solid is built out of the clusters, the molecular levels broaden into bands, which however remain quite narrow in this material. Although the main intercluster hopping occurs via $dd\sigma$ matrix elements (here and below we mean for d the Ru-O molecular orbitals with the effective d symmetry), the intercluster distance is large and the effective hopping amplitude is small. Thus one may conjecture that

the valence band formed out of the majority spin molecular T_{2g} orbitals and the corresponding minority spin band do not overlap, and that the crystal, in either the ferro- or antiferromagnetic states, remains insulating. A more detailed analysis, as discussed later in the paper, reveals a difference between the ferro- and antiferromagnetic ordering, namely, that the bandwidth is slightly larger, and the exchange splitting slightly smaller in the former case. In fact, our LDA calculations, described above, yield an insulating antiferromagnetic ground state, with a small gap of about 0.07 eV; they also give a metastable semimetallic ferromagnetic state, with a band overlap of a few meV.

Let us now analyze this band structure in the tight-binding terms. A nearest-neighbor model should be a good starting approximation. Let us begin with the ferromagnetic case, and consider the undistorted crystal structure (no tilting of oxygen octahedra). The main parameter is now the xy - xy hopping amplitude $\tau_\sigma = 0.75t_{dd\sigma}$. In the nearest-neighbor approximation, the three T_{2g} bands do not hybridize with each other. Each of them, however, disperses according to $E_k = E_+(T_{2g}) + 4\tau_\sigma \cos(k_x a/2) \cos(k_y a/2)$, and the corresponding permutations of x, y, z . Including $dd\pi$ hopping, the bands hybridize among themselves, resulting in a further increase in the bandwidth. The calculated LDA bands have widths of approximately 1.1 eV, corresponding to $\tau_\sigma \approx 0.14$ eV. $dd\pi$ hopping effects are responsible for the deviations from the dispersion above by about 0.1 eV. Importantly, there is no repulsion between the valence bands and the conduction bands, because they are fully spin polarized with the opposite spins. This situation changes, however, in the antiferromagnetic case.

The observed magnetic ordering corresponds to ferromagnetic 001 planes stacked antiferromagnetically. Each RuO_6 cluster has thus four neighbors with the same and eight neighbors with the opposite spin. Correspondingly, of three T_{2g} -derived bands one (xy) remains essentially the same as in the ferromagnet, and two other lose their dispersion to the first order in τ_σ , since the relevant neighboring clusters have only states of the opposite spin at this energy. Instead, for those bands there is a hybridization between the valence and the conduction bands, because now the orbitals with the same spin on the neighboring clusters belong to these different bands. The hybridization matrix element is $t_\sigma(\mathbf{k}) = 4\tau_\sigma \cos(k_{x,y} a/2) \cos(k_z a/2)$, and produces an additional bonding energy $2J \approx \langle t_\sigma^2(\mathbf{k}) \rangle / \Delta$ per cluster ($\Delta \approx 1$ eV is the exchange splitting). This yields about 0.08 eV which is very close to the calculated LDA energy difference (0.12 eV) between the AF and F configurations in the ideal undistorted structure. In the actual crystal structure the oxygen octahedra are tilted by about 12° , so that τ is reduced by about 15% (neglecting τ_π etc.), yielding $2J \approx 0.06$ eV. Our first principles LAPW calculations give for the bandwidth approximately 0.9 eV, that is, $\tau_\sigma \approx 0.11$ eV, and $2J \approx 0.05$ eV. The calculated LAPW energy difference is 0.095 eV, the same reduction from the undistorted case as given by the simple tight-binding estimate above. It is worth noting that while this mechanism gives an effective antiferromagnetic exchange interaction $J \propto \tau^2 / \Delta$, the underlying physics is very similar to, but not identical with, the usual superexchange interaction in $3d$ oxides, $J \propto t^2 / U$. The differences are that instead of metal-oxygen-metal hopping here the relevant

hopping is direct cluster-cluster hopping and the energy denominator is the band gap due mainly to intracluster exchange, rather than Coulomb correlations described by a Hubbard U .

One can also estimate the Néel temperature, using the above value for J . To do that, let us begin with noting that this system represents a very good approximation to the antiferromagnetic nearest-neighbor fcc model. The strong magnetoelastic coupling discussed below does not favor noncollinear spin configurations, and so the direction of the cluster magnetic moments is fixed. The magnetic coupling J_2 with the next-nearest neighbors can be safely neglected. Indeed, it is governed by the $dd\sigma$ hopping. Although τ_σ is larger than τ_π , usually by a factor of the order of 2, the larger distance, in the canonical scaling $d^{l+l'+1}$ gives a factor of $2^{-2.5} = 0.18$, and the energy denominator in the equation for J is about 10 times larger. Taken together, one expects J_2 to be at least two orders of magnitudes smaller than J . The antiferromagnetic fcc Ising model is well studied.⁴² Despite magnetic frustration, it has a Néel temperature of approximately $1.76J$, for the spin 1/2 and approximately $1.33J$, for the spin 1, which in our case corresponds to 700–900 K. The measured T_N is 26 K, in apparent severe disagreement with our estimate.

It is tempting to ascribe this to intracluster Hubbard-like correlation effects, which can increase the gap and reduce J . Moreover, since the t_{2g} bandwidth is only 1 eV, even a moderate Hubbard repulsion could affect J . One can get a very rough upper estimate for this effect as follows: The energy of the Coulomb repulsion of two electrons placed in two t_{2g} orbitals on the same cluster is (assuming about equal population on Ru and O) $U \approx 0.25U_{O-O} + 0.25U_{Ru-Ru} + 0.5U_{Ru-O}$, where U_{O-O} is the Coulomb repulsion of two electrons localized on two neighboring oxygens, etc. $U_{O-O} \approx 1/d_{O-O} = 4.4$ eV; U_{Ru-Ru} is believed to be about 1.5 eV,²⁴ and for U_{Ru-O} we use 3 eV, keeping in mind that the charge-transfer metal-oxygen energy for the $3d$ oxides is about 4.5 eV and the metal-oxygen distance is 50% smaller there. Then, we arrive at $U < 3$ eV. It is unclear to what extent this U will be reduced by screening by surrounding cluster and by intracluster charge redistribution, but this effect would definitely be substantial. Anyway, using 3 eV as a very safe upper bound, we get for the lower bound on $2J$ approximately 0.03 eV, which corresponds to T_c of at least 300 K. Thus, strong correlations alone cannot explain anomalously low Néel temperature of this compound. Another possibility to reduce the transition temperature is magnetoelastic coupling, which is subject of the next section.

3. Magnon-phonon coupling

The fact that magnetic excitations and phonons are coupled in ruthenates is known,² but not well understood from a microscopic point of view. In the case of Sr_2YRuO_6 it is, however, reasonably clear: With increasing tilting angle the τ_σ hopping must decrease and with it the antiferromagnetic stabilization energy and effective exchange constant J . This is confirmed by our first principles results. In other words, magnetic excitations flipping the spin of a RuO_6 cluster are coupled with this phonon mode, changing the tilting angle (which is the soft mode for the transition

from the cubic structure into the tilted one). A dimensionless coupling constant may be defined as $\lambda = d \ln J / dQ$, where $Q = u_O \sqrt{2M_O \omega / \hbar}$ is the phonon coordinate. Here u_O is the displacement of oxygens from their equilibrium positions, and ω is the frequency of the phonon. Very roughly, $M_O \omega^2 = 8\Delta E / d^2$, where ΔE is the energy difference between the cubic and the distorted structure, taken per one oxygen, and d is the equilibrium oxygen displacement. From our calculations, $\Delta E = 90$ meV. Experimentally, $d \approx 0.4$ Å. Thus, $\omega \approx 270$ cm⁻¹. Now, using $2J \propto \tau_\sigma^2 \propto \cos^2 2\theta$, where θ is the tilting angle, we can estimate $d \ln J / du_O \approx 8\theta_0^2 / d \approx 0.8$ Å⁻¹. In fact, linear interpolation of J between the cubic and equilibrium structure gives the same number for $d \ln J / du_O$. Thus λ is about 0.17 for this phonon mode, which means that the characteristic (e.g., zero-point motion) amplitude of the librations of the octahedra around their equilibrium position will produce sizable changes in the effective exchange constant. The thermodynamics of such a system is interesting and unusual, but its discussion goes beyond the scope of this paper. It is important to note, however, that the long-range order in the nearest-neighbor antiferromagnetic fcc Ising model appears exclusively because of the finite-temperature entropy contribution to the free energy.⁴³ While at $T=0$ there is an infinite number of degenerate states, ordered in two dimensions and disordered in the third one, at $T>0$ this degeneracy is lifted because of different spectra of low-energy spin-flip excitations in the different ground states. As long as such spin-flip excitations are coupled with the phonons, the standard consideration of the AF fcc Ising model does not apply, and the transition is not necessarily at $T \approx J$. However, the long-range two-dimensional AF correlations should be present up to $T \approx J$, and could in principle be seen in some experiments.

4. Extended Stoner model for Sr_2YRuO_6

The above discussion of Sr_2YRuO_6 magnetic properties was based on the molecular (cluster) picture, and we observed that oxygen plays a crucial role in formation of the magnetic state. The same conclusion can be obtained, starting from the extended band picture. The standard approach to magnetism in the band theory goes back to Slater⁴⁴ and Stoner.⁴⁴ They considered noninteracting electrons in the paramagnetic state, and added their exchange interaction in an average form, $H_{\text{mag}} = In_\uparrow n_\downarrow = \text{const} - Im^2/4$, where m is total magnetization and I is independent of m . The magnetic susceptibility of such a system can be written as

$$\chi^{-1} \equiv \partial^2 E / \partial n_\uparrow \partial n_\downarrow = \chi_0^{-1} - I, \quad (1)$$

where χ_0 is the Pauli susceptibility. If magnetization is measured in Bohr magnetons, then $\chi_0 = N(0)$, the density of states per spin at the Fermi level. The instability occurs when χ diverges, that is, when $IN(0)$ becomes larger than 1. Equation (1) can of course be viewed as an approximation in the framework of the general linear response theory. However, such an approximation is highly uncontrollable, and even the splitting of the right-hand part of Eq. 1 into two terms cannot be derived in a systematic way. More instructive is application of the Stoner method to the density functional theory (DFT). In DFT, total energy change is exactly written as sum of the change in the one-electron energy,

which for small m is $N(0)^{-1}m^2/4$, and the change in the interaction energy, which is $(\partial h/\partial m)m^2/4$. Here $h = \langle V_{\uparrow} - V_{\downarrow} \rangle$ is the effective Kohn-Sham magnetic field averaged over the sample (because Stoner theory assumes a uniform internal ferromagnetic field), and $I \equiv -(\partial h/\partial m)$.

The utility of the Stoner approach in DFT is due to the fact that usually there are very few orbitals whose occupancy substantially influences h , and therefore I is easy to calculate in a quasiatomic manner, using, for instance, the quasiatomic loop in standard LMTO codes. In practice, in quasiatomic calculations one changes the occupation of a given orbital, transferring some charge from the spin-up to spin-down quasiatomic level, recalculates the LSDA potential and determines how large the induced splitting of quasiatomic levels is.

If different kinds of atoms in a solid contribute to the density of states at the Fermi level, one has to take into account the magnetization energy for each of them. This means that the total Stoner I for such a solid is the average of the individual (quasiatomic) I 's with the squared partial density of states. Indeed, suppose the states at the Fermi level are a superposition of orbitals from several atoms, so that $N(0) = \sum_i N_i = N(0) \sum_i \nu_i$ (where i labels the atoms). Applying a uniform magnetic field creates a magnetization $m = \sum_i m_i$, where $m_i = \nu_i m$ is magnetization of the i th atom. By definition, the intraatomic energy change is $-\sum_i I_i m_i^2/4 = -\sum_i I_i \nu_i^2 m^2/4$. Thus, the total $I = \sum_i I_i \nu_i^2$.

So formulated, the Stoner theory applies to infinitesimally small changes in magnetization and essentially determines whether or not the paramagnetic state is stable against ferromagnetism. It is, however, a reasonable assumption that this theory holds, approximately, for finite magnetizations as well. One has, however, to modify the one-electron energy term $N(0)^{-1}m^2/4$, to account for the energy dependence of the density of states, within the rigid-band approximation. Then, the spin splitting producing a given magnetization m can be defined as $\Delta = m/\bar{N}(m)$, where $\bar{N}(m)$ is the density of states averaged between the Fermi level of the spin-up and spin-down subbands. For the one-electron energy one obtains $\partial E_1/\partial m = m/2\bar{N}$, because one has to move $m/2$ electrons up by Δ . Integrating this expression, one arrives at the so-called extended Stoner theory,⁴⁵ which uses the following expression for the total magnetization energy:

$$E(m) = \frac{1}{2} \int_0^m \frac{m' dm'}{\bar{N}(m')} - \frac{Im^2}{4}. \quad (2)$$

Minimization of this energy leads to the extended Stoner criterion, which states that stable (or metastable) values of the magnetic moment are those for which $\bar{N}(m)I = 1$ and $d\bar{N}(m)/dm < 0$. The paramagnetic state is (meta)stable when $\bar{N}(0) \equiv N(0) < 1/I$.

Stoner theory is, in principle, formulated for a ferromagnetic instability. However, unless the Fermi surface topology specifically favors (or disfavors) the antiferromagnetic instability with a given vector \mathbf{Q} , one can assume that $\chi_0(\mathbf{Q}) \approx \chi_0(0)$. Indeed, in many cases if a material comes out magnetic from the calculations, the energy difference between ferro- and antiferromagnetic ordering is small compared with the magnetic stabilization energy. As we shall

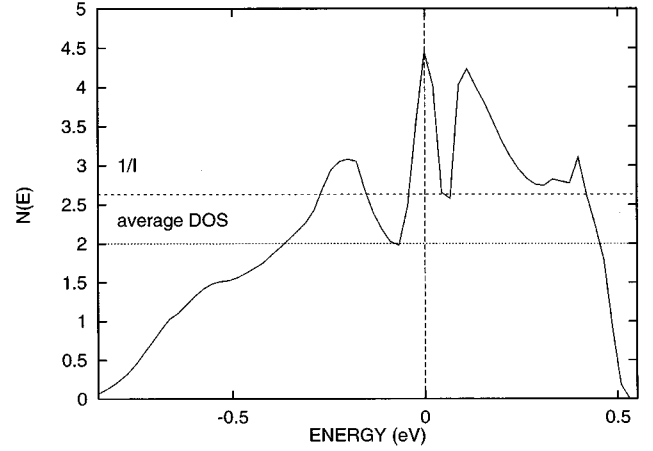


FIG. 5. LMTO density of states of the T_{2g} band of the nonmagnetic Sr_2YRuO_6 and inverse Stoner parameter $1/I$.

see, this is the case in Sr_2YRuO_6 , but not in SrRuO_3 , and the reason is that in the latter the Stoner factor I is very different for ferro- and antiferromagnetic arrangements.

Now let us consider how one can describe the magnetism in Sr_2YRuO_6 from the Stoner point of view. Calculation of Stoner parameters I 's is straightforward in the LMTO method,⁴¹ which divides space into atomic spheres. In the popular Stuttgart LMTO-TB package it is possible to change occupancy of any atomic orbitals and to calculate the resulting change in atomic parameters, in particular the shift of the corresponding band center C_{li} . With the spin-up and spin-down occupancies split by $\pm m/2$, the Stoner parameter is $(C_{\uparrow} - C_{\downarrow})/m$. We obtain I_{Ru} of about 0.7 eV and, importantly, find that the O_p states in ruthenates also have substantial Stoner parameter, $I_{\text{O}} \approx 1.6$ eV. The density of the Ru d states is approximately twice larger than that of the three O p states. Thus, the total Stoner parameter for Sr_2YRuO_6 is $I = I_{\text{Ru}}\nu_{\text{Ru}}^2 + 3I_{\text{O}}\nu_{\text{O}}^2 \approx 0.38$ eV. Correspondingly, the paramagnetic state is unstable unless $N(0) < 2.6$ states/(spin-eV-formula). The paramagnetic LMTO density of states of cubic Sr_2YRuO_6 (that is, with breathing, but with no tilting distortion) near the Fermi level is shown in Fig. 5.

It has the narrow T_{2g} band half filled, and $N(0)$ is close to 4.5 states/spin eV formula. This is much larger than $1/I$, and so the paramagnetic state is very unstable. On the other hand, the average density of states in the T_{2g} band is not that large, $\bar{N} \sim 3/W \approx 3/1.5 \text{ eV} = 2$ states/spin eV, thus in the cubic structure this band will not be fully polarized.

Integrating the density of states shown in Fig. 5, we obtain the extended Stoner plot for Sr_2YRuO_6 (Fig. 6), and observe that the equilibrium magnetization is slightly smaller than $2\mu_B$, and the ground state is semimetallic, in agreement with the self-consistent spin-polarized LMTO calculations, as well as with the more accurate LAPW calculations. Another fact that one can observe from Fig. 6 is that if oxygen would not contribute in the total Stoner factor, that is, if the total I were only $I_{\text{Ru}}\nu_{\text{Ru}}^2 \approx 0.31$ eV, equilibrium magnetization would be very small, approximately $0.4\mu_B$, and of course with a much smaller gain in energy. As we shall see below, this is the case in SrRuO_3 , where in the antiferromagnetic structure oxygen ions cannot polarize by symmetry.

In Sr_2YRuO_6 , however, oxygen fully contributes into the

magnetic stabilization energy both in ferro- and in antiferromagnetic structure, and so the next-order mechanisms decides which magnetic order realizes. Such an additional mechanism is discussed in the previous section hybridization repulsion between the filled and the empty T_{2g} bands, which stabilizes the antiferromagnetic structure.

B. SrRuO₃ and CaRuO₃

1. Tight-binding bands and relation to Sr₂YRuO₆

The main structural difference from the double perovskite Sr₂YRuO₆ is that now all oxygen ions are shared between

two rutheniums, and so one cannot make use of a single RuO₆ cluster concept. As with Sr₂YRuO₆, we shall start by analyzing the band structure with nontilted octahedra, that is, with the cubic perovskite structure. Per cubic cell we have, in each spin channel, two Ru e_g states, strongly hybridized with 3 O p_σ orbitals, and three Ru t_{2g} states, hybridized with 6 O p_π orbitals. In the nearest-neighbor approximation, these $pd\sigma$ bands do not mix with the $pd\pi$ bands, and the $pd\pi$ bands, in turn, consist of three sets of mutually noninteracting xy , yz -, and zx -like bands. The nearest-neighbor TB Hamiltonians have the form

$$H(e_g) = \begin{pmatrix} E_0(e_g) & 0 & 2t_\sigma s_x/\sqrt{3} & 2t_\sigma s_y/\sqrt{3} & 4t_\sigma s_z/\sqrt{3} \\ 0 & E_0(e_g) & 2t_\sigma s_x & -2t_\sigma s_y & 0 \\ 2t_\sigma s_x/\sqrt{3} & 2t_\sigma s_x & E_0(p_\sigma) & 0 & 0 \\ 2t_\sigma s_y/\sqrt{3} & -2t_\sigma s_y & 0 & E_0(p_\sigma) & 0 \\ 4t_\sigma s_z/\sqrt{3} & 0 & 0 & 0 & E_0(p_\sigma) \end{pmatrix}$$

and

$$H(xy) = \begin{pmatrix} E_0(t_{2g}) & 2t_\pi s_x & 2t_\pi s_y \\ 2t_\pi s_x & E_0(p_\pi) & -4t'_\pi s_x s_y \\ 2t_\pi s_y & -4t'_\pi s_x s_y & E_0(p_\pi) \end{pmatrix},$$

where $s_x = \sin(k_x a/2)$, etc. For each t_{2g} manifold three bands appear: one nonbonding at $E_0(p_\pi)$ and one bonding-antibonding pair at $E_\pm(xy) = 0.5\{E_0(p_\pi) + E_0(t_{2g}) \pm \sqrt{[E_0(p_\pi) - E_0(t_{2g})]^2 + 16t_\pi^2(s_x^2 + s_y^2)}\}$. Analysis of the calculated band structure shows that $E_0(t_{2g}) \approx E_0(p_\pi)$, and so, neglecting oxygen-oxygen hopping t' , the dispersion is approximately $E_0(t_{2g}) \pm 2t_\pi \sqrt{s_x^2 + s_y^2}$, where $t_\pi \approx 1.4$ eV. Ru e_g orbitals are split off from the t_{2g} orbitals by about 3 eV. As in Sr₂YRuO₆, the crystal field effect on oxygen states is weaker: The O p_σ states are less than 2 eV below O p_π states. The energy distance between Ru e_g and O p_σ levels is nearly 5 eV, and so a good approximation is $\Delta E = E_0(e_g) - E_0(p_\sigma) \gg t_\sigma$. Applying Löwdin perturbation theory to fold down the oxygen states, we get for (antibonding) E_g bands the effective Hamiltonian

$$H(e_g) = \begin{pmatrix} E_0(e_g) + 4t_\sigma^2(s_x^2 + s_y^2 + 4s_z^2)/3\Delta E & 4t_\sigma^2(s_x^2 - s_y^2)/\sqrt{3}\Delta E \\ 4t_\sigma^2(s_x^2 - s_y^2)/\sqrt{3}\Delta E & E_0(e_g) + 4t_\sigma^2(s_x^2 + s_y^2)/3\Delta E \end{pmatrix},$$

which yields two bands with dispersion $\epsilon_k = E_0(e_g) + 8t_\sigma^2(s_x^2 + s_y^2 + s_z^2 \pm \sqrt{s_x^4 + s_y^4 + s_z^4 - s_x^2 s_y^2 - s_z^2 s_x^2 - s_z^2 s_y^2})/\Delta E$.

The formal valency of Ru in Sr_xCa_{1-x}RuO₃ is 4. The total number of electrons, populating the Ru-O valence bands, is 22. This means that the bonding (mostly oxygen) E_g bands are filled, as well as the bonding and nonbonding T_{2g} bands. The conduction band is the antibonding T_{2g} band, with its six states filled by four electrons. This band has a strong (logarithmic) van Hove singularity at half filling. However, direct oxygen-oxygen hopping $t' \approx 0.3$ eV, which we have initially neglected, moves this singularity upwards to the position which corresponds to approximately 63% filling (3.8 electrons) and makes the singularity sharper. This is the pronounced peak at E_F in our first principles paramagnetic DOS.⁶ Such a situation, where the Fermi level nearly exactly hits a logarithmic peak in the density of states, is

energetically unfavorable, and leads to an instability, which can be either magnetic, or a sufficiently strong lattice distortion, or both.

2. Cubic perovskite: Magnetic instability

The calculated partial densities of Ru (d) and of the three O (p) states at the Fermi level in Sr_xCa_{1-x}RuO₃ are approximately 70% and 30%, respectively. Correspondingly, $I = I_{\text{Ru}}\nu_{\text{Ru}}^2 + 3I_{\text{O}}\nu_{\text{O}}^2 \approx 0.41$ eV. Without the oxygen Stoner parameter, $I \approx 0.35$. As mentioned above, our LAPW calculations yield for SrRuO₃ in the cubic structure a relatively small magnetization of $1.17\mu_B$. The reason for that is that the density of states is piled near the Fermi level, and drops quickly when one goes away from it. Figure 8, below, shows how this is reflected in the effective density of states

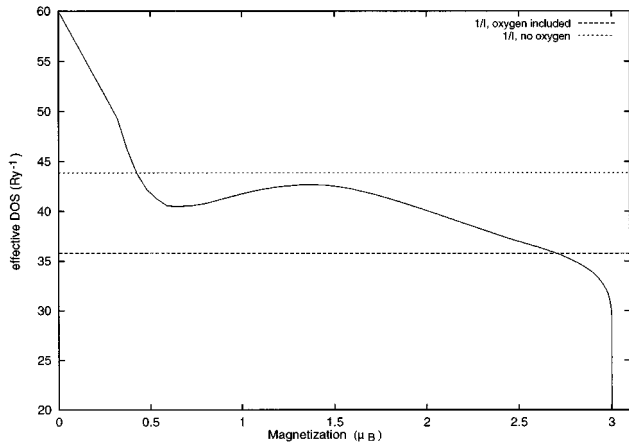


FIG. 6. Extended Stoner plot for the density of states shown on Fig. 5.

$\tilde{N}(m)$: It decreases rapidly with magnetization, and becomes equal to $1/I$ at $m \approx 1.2\mu_B$. For a moderate tilting, corresponding to actual SrRuO_3 structure, $\tilde{N}(0)$ is smaller than in the cubic structure, but it decreases rather slowly with m and remains larger than $1/I$ much longer.

Two questions arise in this connection: Why is the ground state is ferromagnetic, and not antiferromagnetic, and why in the actual crystal structure is CaRuO_3 not magnetic at all? The first question is particularly easy to answer. In an antiferromagnetic structure, oxygen ions occur between opposite spin Ru ions, and thus by symmetry have zero net polarization. Correspondingly, the total Stoner parameter I is smaller and so is magnetic stabilization energy and the equilibrium magnetization on Ru. As we shall see below, tilting has a substantial effect on the effective density of states, and for large tiltings the ground state becomes paramagnetic. It follows from the above discussion, however, that the ground state is always either ferro- or paramagnetic.

This situation is in sharp contrast with classical localized magnetic materials, like NiO or FeO, where even when ferromagnetism is imposed, oxygen is polarized only very weakly, and the magnetization of the metal ion is even smaller than for the antiferromagnetic state. It is also in contrast with the ferromagnetic colossal magnetoresistance Mn

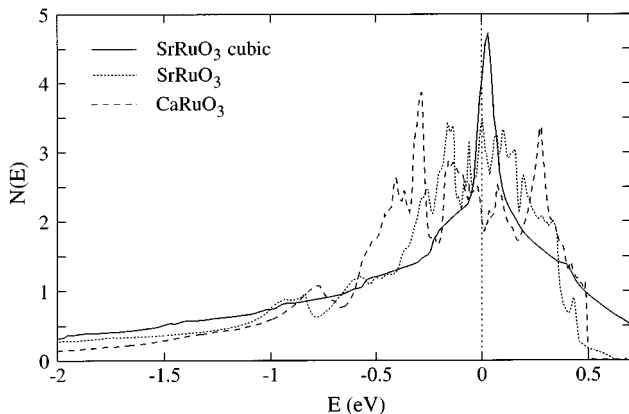


FIG. 7. LAPW densities of states in the T_{2g} band in SrRuO_3 in the cubic and its actual structure, and of CaRuO_3 in its actual structure, and with experimental lattice parameters (4% smaller for CaRuO_3).

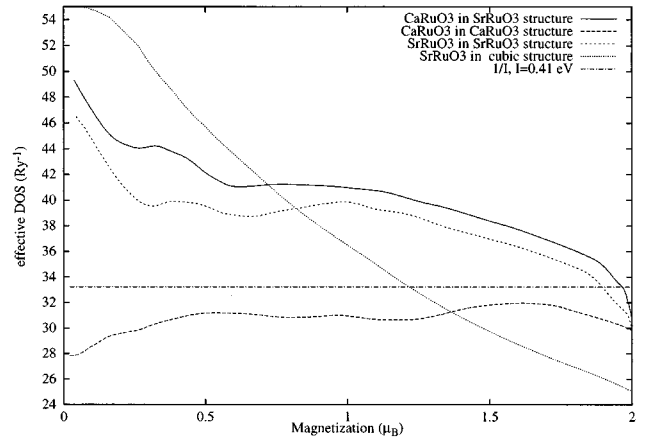


FIG. 8. Extended Stoner plot for SrRuO_3 and CaO_3 in various structures, produced with the densities of states shown in Fig. 7. Inverse Stoner factors are calculated in the LMTO atomic spheres as described in the text.

oxides, where the antiferromagnetic ground state is destroyed by the double-exchange interaction, competing with superexchange. These ruthenates have integer occupancy of the valence band, and thus double exchange is not operative. However, covalency effects, which are strong because of the large pd hopping and the near degeneracy of the Ru (t_{2g}) and O (p_π) states, are operative. This strong covalency is what requires part of the magnetic moment to reside on the oxygen, since exchange splitting the Ru d states without the O would require disrupting the covalent bonding.

In the crystal structures where it is possible to maintain O moments without ferromagnetic ordering, an antiferromagnetic state is likely to form (as in Sr_2YRuO_6), but where it is not possible, like SrRuO_3 , a ferromagnetic ground state occurs instead. It is also worth noting that besides the double perovskite Sr_2YRuO_6 , where oxygen ions can polarize both in the ferro- and antiferromagnetic structure, and single perovskites $\text{Sr}_x\text{Ca}_{1-x}\text{RuO}_3$, there exist intermediate layered structures, which consist of perovskite $(\text{Sr,Ca})\text{O}_2$ layers. Using the same arguments, we conjecture that if such compounds are magnetic, the effect of oxygen will cause ferromagnetic ordering inside layers, while interlayer coupling is strong ferromagnetic if the layers are sharing apical oxygens, but may be antiferromagnetic if they are connected by intermediate rocksalt layers (like in Sr_2RuO_4).

3. Role of the orthorhombic distortion

The observed crystal structure of both SrRuO_3 and CaRuO_3 is characterized by a substantial tilting of the RuO_6 octahedra. In SrRuO_3 the octahedra are rotated by 8° , and in CaRuO_3 the distortion is about twice larger. In Fig. 7 we show the density of states in the T_{2g} band for these three different structures. There are two interesting effects on the electronic structure, associated with tilting. One is that hybridization between the T_{2g} and E_g bands becomes possible. This broadens the logarithmic singularity in the density of states. At the same time the bands become more narrow and the gap between the antibonding T_{2g} and E_g bands grows. On the other hand, the unit cell is quadrupled so new Bragg reflections appear. These yield pseudogaps at the new Brillouin zone boundaries, occurring at energies close to half

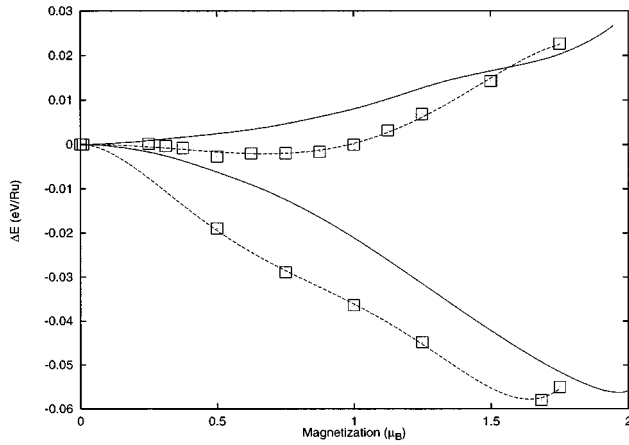


FIG. 9. Ferromagnetic stabilization energy for CaRuO_3 in its actual crystal structure and in the SrRuO_3 crystal structure. First principles LAPW fixed-moment calculations (squares; the dashed lines are guides to eye) are shown together with the approximate Stoner formula [Eq. (2)], based on the data shown in Fig. 8.

filling (e.g., along ΓX and ΓM directions) as well at two-third filling (e.g., along ΓR direction). This second pseudogap thus appears to be near the Fermi level. One factor, band narrowing, tends to increase the equilibrium magnetization, but another one, the second pseudogap at the Fermi level, works against it. The actual trend looks like this: At small distortions the equilibrium magnetization grows. At some critical distortion magnitude, which is not far from the observed equilibrium distortion for SrRuO_3 , the magnetization reaches a maximum and starts to decline. The first principles calculations show little difference between SrRuO_3 and CaRuO_3 , provided the same crystal structure is used, and so the main difference in the observed behavior is indeed due to the different distortion magnitudes.

To understand the changes caused by the tilting distortion it is instructive to look at the extended Stoner plots for different distortions. Figure 8 shows such plots for SrRuO_3 in the experimental structure, in the cubic (ideal perovskite) structure, and for CaRuO_3 , as well as for CaRuO_3 in the SrRuO_3 structure. One may immediately note the extreme instability of the cubic structure, due to discussed peak at the Fermi level. However, because the density of states is piled up near the Fermi level, the resulting exchange splitting is small compared with the bandwidth. For the moderate tilting, like that in the experimentally observed SrRuO_3 structure, the peak broadens and it takes larger exchange fields to fully split this peak into occupied and unoccupied peaks. Finally, at even larger tiltings, corresponding to CaRuO_3 , the peak is suppressed. In the effective density of states, as shown in Fig. 8, this results in a nearly flat plateau, extending from $m=0$ to $m \approx 1 \mu_B$. Accidentally, this plateau matches nearly exactly $1/I$, calculated as described in the previous section. In other words, the total energy of CaRuO_3 is nearly independent of magnetization up to $m \approx 1 \mu_B$. The total energy as a function of magnetization is shown in Fig. 9, where the results of the fixed-spin-moment LAPW calculations are compared with the same energy differences in the Stoner theory.⁴⁶

We conclude that although CaRuO_3 is nonmagnetic in its ground state, long-wave paramagnons should be extremely

soft in this compound. This should effect the transport, magnetic and electronic properties.

4. Transport properties

Unusual transport properties of SrRuO_3 are due to the following three peculiarities: (1) While the DOS in both spin subsystems are nearly the same, the partial plasma frequency in the majority spin channel is 3 times larger than in the minority spin channel, a manifestation of the proximity to the half-metallic regime, which would occur if the magnetization were $2 \mu_B$ instead of $1.59 \mu_B$. (2) There is strong coupling between electrons, phonons, and magnons, which probably produces substantial spin-flip scattering of electrons. And (3) in both spin channels the Fermi surfaces consist of several sheets of complicated topology: holelike, electronlike, and open, so that holelike and electronlike parts compensate each other.

Let us start with the electric resistivity, and assume for simplicity that two bands are present, spin up and spin down. Let us further assume that the sources of the resistivity are scattering of electrons by phonons, with the coupling constant $\lambda_{\text{ph}\uparrow} = \lambda_{\text{ph}\downarrow} = \lambda_{\text{ph}}$, and by magnons, with the coupling constant λ_m . Since the DOS are approximately equal, $N_{\uparrow} = N_{\downarrow} = N \approx 23$ st/Ry, also $\lambda_{\uparrow\downarrow} = \lambda_{\downarrow\uparrow} = \lambda_m$. The specific heat renormalization in each band is now $(1 + \lambda_{\text{ph}} + \lambda_m)$ which would need to be ≈ 4.0 to agree with experiment.²⁷ In the lowest-order variational solution of the Boltzmann equation, given by Pinski *et al.*⁴⁷ (see also Ref. 48), the resistivity of such a system at sufficiently high temperature is $\rho = 8 \pi^2 k T (\lambda_{\text{ph}} + \lambda_m) / \omega_p^2$, where the so-called “scattering-in” term which is usually small in cubic crystals is neglected, and $\omega_p^2 = \omega_{p\uparrow}^2 + \omega_{p\downarrow}^2$ is the partial plasma frequency squared. (One can find in the literature⁴⁹ a so-called “two-current formula” which gives the same result when the “scattering-in” term is neglected. There are some differences between the formulas of Refs. 47 and 49, which we discuss in the Appendix.)

From our first principles calculations, $\omega_{p\uparrow} = 3.3$ eV and $\omega_{p\downarrow} = 1.5$ eV. In the nonmagnetic phase $\omega_p = 6.2$ eV, the same as the total plasma frequency in the ferromagnetic phase. At $T \gtrsim 30$ K and up to the Curie temperature the resistivity is reported to be linear.²⁷ The linear coefficient ($\sim 1 \mu\Omega \text{ cm/K}$) corresponds to $(\lambda_{\text{ph}} + \lambda_m) \approx 2.9$, very close to the number extracted from the electronic specific heat. Above T_C the resistivity changes slope, remaining linear up to at least several hundred kelvin. The slope is, however, smaller than below T_C , and corresponds to $\lambda = \lambda_{\text{ph}} + \lambda_{\text{pm}} \approx 1.5$, where λ_{pm} is the electron-paramagnon coupling constant. This value differs from that quoted in Ref. 27, because of considerable differences in the calculated band structure. Thus, we conclude that the high-temperature resistivity of SrRuO_3 indicates rather strong electron-paramagnon, and even stronger electron-magnon coupling, with the reservation that probably in this system one cannot really separate electron-phonon and electron-magnon scattering completely because the corresponding degrees of freedom are coupled. The problem noted in Ref. 27, namely, that at high temperatures the mean free path is comparable to the lattice parameter, yet no saturation is seen in the resistivity, remains.

The resistivity of CaRuO_3 has also been studied. In the studies reported in the literature^{1,13,50} the high-temperature resistivity shows the same slope as in SrRuO_3 , in full agreement with our observation that the electronic structure of both compounds is very similar. At low temperatures, however, the resistivity behaves very differently; namely, it increases nearly linearly at small T with a large slope. The slope decreases eventually and at the room temperature the behavior becomes similar to that of SrRuO_3 . This low-temperature linearity indicates that the excitations responsible for resistivity (apparently, paramagnons) soften at $T \rightarrow 0$, indicating a magnetic instability at $T=0$ or at slightly negative T (in Curie-Weiss sense). This is in agreement with our result that CaRuO_3 is on the borderline of a ferromagnetic state. Again, paramagnons are strongly coupled with phonons, and this leads to the large coupling strength.

The low-temperature resistivity has also attracted attention. Experimentally, the resistivity initially increases rather quickly. Allen *et al.*²⁷ observed a low-temperature power law $\rho(T) - \rho(0) \propto T^{1-2}$. Klein *et al.*¹⁵ found that below 10 K the resistivity can be reasonably well fit with a quadratic law, but an even better fit (linear), was found for up to 30 K for the dependence of resistivity on magnetization. We interpret this observation as follows: A stronger than T^5 increase indicates that the excitations, responsible for the low-temperature scattering, have a sublinear dispersion. Conventional magnons, with $\omega \propto k^2$ dispersion, produce $\rho \propto T^2$, in good agreement with the experiment. In fact, the experimental exponent is even below 2, which is easily accountable for by the Fermi surface effects: Part of the temperature dependence comes from the term $(\mathbf{v}_k - \mathbf{v}_{k'})^2$, if it is proportional to $(\mathbf{k} - \mathbf{k}')^2$; this not the case in SrRuO_3 , where one of the two Fermi surfaces (majority spin) is a small sheet with heavy electrons (similarly, magnetic alloys where momentum conservation does not hold show $\rho \propto T^{3/2}$; see Ref. 51). A possible problem with this interpretation of the low-temperature resistivity is that as was already noted,¹⁵ in elemental ferromagnets, the magnon-limited resistivity is almost three orders of magnitude smaller than what would be needed to explain the low-temperature resistivity of SrRuO_3 (where $\rho \rightarrow \rho_0 + aT^2$, $a \approx 0.02 \mu\Omega \text{ cm/K}^2$). This can be resolved if we invoke the anomalously large magnon-phonon coupling, which, as discussed above, originates from the crucial role played by oxygen in magnetic properties of ruthenates. The strong electron-magnon coupling at low temperature in SrRuO_3 is closely related to the large electron-paramagnon coupling at high temperatures and in CaRuO_3 . One can make a rough estimate of the characteristic frequency of magnons responsible for the resistivity: The Schindler-Rice formula,⁵² derived for the s - d paramagnon scattering, should be qualitatively applicable here, because we also have light electrons which carry current and are scattered by magnons into a heavy, transport-inert band. This formula reads

$$\rho(T) \approx \alpha (T/T_m)^2 [J_2(T_m/T) - (T/T_m)^3 J_5(T_m/T)],$$

$$J_n(x) = \int_0^x \frac{4z^n dz}{\sinh^2(x/2)},$$

and has asymptotic behavior at $T \rightarrow 0$ as $\alpha (T/T_m)^2 \pi^2/3$ and at $T \gg T_m$ as $\approx 0.8\alpha (T/T_m)$, where kT_m is characteristic en-

ergy of the magnons. Using the experimental number $(\rho - \rho_0)/T^2 \approx 0.02 \mu\Omega \text{ cm/K}^2$ and assuming that the magnon-limited part of the high-temperature resistivity is $\sim 0.5 \mu\Omega \text{ cm/K}$, we arrive at $T_m \sim 70$ K, which is a low, but not impossible number.

The Hall coefficient in SrRuO_3 and CaRuO_3 (Ref. 12) has attracted considerable attention. In both compounds the Hall constant R shows an unusual temperature dependence, changing sign at $T \sim 50$ K. At this point, however, the similarity ends. For each given temperature the Hall resistivity ρ_{xy} in CaRuO_3 is nearly perfectly proportional to the field, as it should be for ordinary Hall processes. In SrRuO_3 , to the contrary, $d\rho_{xy}/dH$ decreases substantially with temperature, and only well above T_c does ρ_{xy} become a linear function of H . This closely resembles the so-called extraordinary Hall effect in ferromagnets.

The physics of the extraordinary Hall effect is as follows: Below T_c , the internal magnetic field is much larger than that applied in a typical Hall experiment. However, the Hall currents induced in different magnetic domains mutually cancel. The applied field acts by aligning domains and lifting this cancellation. This process defines the large slope of $d\rho_{xy}/dH$ in low fields. At a field close to the saturation magnetization $4\pi M_s$ all domains are aligned and further change of the Hall current is due to the applied field itself (the ordinary Hall effect). It is tempting to associate the nonlinear field dependence of the Hall resistivity in SrRuO_3 with this effect. However, this hypothesis has been discounted by the authors of Ref. 12 for the following reason: In standard extraordinary Hall effect theory the intersection of the linear low-field and high-field asymptotes occurs at $4\pi M_s$. In SrRuO_3 the position of the intersection is roughly the same for all temperatures below T_c , and falls between 3 and 4 T. Magnetometer data show that $4\pi M_s$ is about 0.12 T at $T=5$ K, and, naturally, drops to zero at $T=T_c$. Furthermore, a closer look at the data reveals that the slope of the Hall coefficient changes in a smooth manner, unlike conventional ferromagnets, where it changes rather sharply near $H=4\pi M_s$.

Studies of the bulk magnetization in polycrystalline⁷ and single crystal³³ samples of SrRuO_3 show that the magnetization is not saturated even at applied fields of several T. This has been ascribed to the strong magnetocrystalline anisotropy, as measured by Kanbayashi,³³ and expected for a $4d$ magnet. Although hysteresis measurements for the thin film samples on which Hall measurements were taken apparently showed saturation near 1.5 T, we speculate that the domains may not yet be fully aligned at this field, yielding a continuing nonlinear field dependence in the Hall resistivity.

The sign reversal of the Hall conductivity has received even more attention. In the literature two explanations can be found: One²⁷ assumes different temperature dependences for the electron and hole scattering rates, because of the different scattering mechanism (phonon vs magnon), which may then yield a strong temperature dependence of the Hall resistivity, and a sign change. It has been argued¹² that this hypothesis should not work, since CaRuO_3 is nonmagnetic, but still shows a sign-changing Hall effect. Instead the authors of Ref. 12 suggested that the sign may change because the number of electrons and holes in the energy window $\sim kT$ around the Fermi energy may change with T . However, the sign

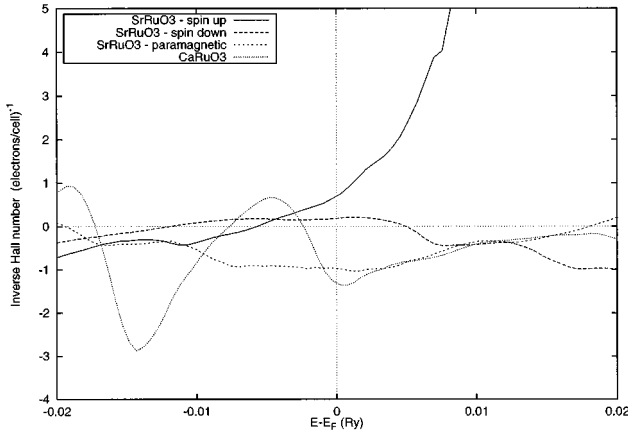


FIG. 10. Calculated inverse Hall number for SrRuO₃ (ferromagnetic and nonmagnetic) and for CaRuO₃. Note different signs for the two spin subbands in SrRuO₃ and strong dependence on the position of the Fermi level.

reversal in CaRuO₃ and SrRuO₃ could be due to different physical reasons. This possibility is also suggested by the very different field dependence of the Hall resistivity in the two cases. On the other hand, it follows from our calculations, and is also indicated by various experiments, that CaRuO₃ is on the verge of a magnetic instability, and the interplay between the phonons and paramagnons may play much the same role as the interplay between the phonons and magnons in SrRuO₃. Furthermore, besides the temperature dependence of the relaxation rates and the temperature broadening of the Fermi level, there is yet another effect which may cause the sign change in SrRuO₃. The exchange splitting must be very temperature dependent in SrRuO₃. Unlike common ferromagnets like Fe, where the Curie temperature corresponds to disordering of local moments, here the magnetization *disappears at T_c*, including the *local* magnetization. Thus, the spin splitting changes with the temperature, essentially disappearing around T_c. This is in contrast with most ferromagnets where an effective local spin splitting exists well above T_c, without any macroscopic magnetization. Thus, the band structure itself is strongly temperature dependent. This effect can be operative in SrRuO₃ in addition to the two other possible mechanisms.

The prerequisite for any of these mechanisms to be relevant is that there is strong compensation between the holelike and the electronlike contributions from the different bands. To check this, we have calculated the Hall conductivity σ_H and the Hall coefficient $R_H = \sigma_H / \sigma_0^2$ for all the individual bands in SrRuO₃ and CaRuO₃, following the procedure described in Ref. 53. The results are shown in Fig. 10. It was observed by Schultz *et al.*⁵³ that quantitative calculations of the Hall coefficient are extremely sensitive to sampling of the Brillouin zone; it is impractical for these 20 atom per unit cell structures to calculate the first principles band structure at a \mathbf{k} mesh comparable with the ultradense meshes used in Ref. 53 for elemental metals and instead we have relied on interpolation between first principles band energies calculated at 100 points in the irreducible wedge of the zone. Thus, our calculations shown in Fig. 10 cannot be taken quantitatively, but rather illustrate the qualitative fact that the Hall conductivity has different signs in different bands and

spin channels. The net Hall conductivity is defined by strong cancellation of holelike and electronlike contributions from different bands so which in turn is very sensitive to relative position of different bands. Evidently, this balance can be easily violated by such temperature-dependent factors as lattice distortion, magnetization, and relaxation times. The mechanism suggested by Gausepohl *et al.*¹² is also possible, since the net Hall conductivity does change sign within a few hundred K around E_F . Finally, very recent measurements⁵⁴ of the Hall coefficient in mixed Sr_xCa_{1-x}RuO₃ samples showed that for intermediate concentrations it does not change sign with temperature, suggesting that the sign reversals in pure compounds are accidental and unrelated.

IV. CONCLUSIONS

At this time there is already a fairly substantial body of experimental literature on these ruthenates, including magnetic measurements, spectroscopic studies, specific heat data, and determinations of electronic transport and superconducting properties. These measurements demonstrate unusual and perhaps unexpected properties, and many of these have been ascribed to correlation effects. For example, the specific heats in the metallic compounds show substantial enhancements over the bare band structure values, superconductivity occurs in a layered material in apparent proximity to magnetic phases, quasiparticle bands measured by ARPES show weaker dispersion than band structure calculations, satellites are observed in angle-integrated photoemission spectra, and the transport properties of the metallic phases are unusual, showing, e.g., sign reversals in the Hall coefficient. Since this evidence clearly suggests something unusual about the perovskite-derived ruthenates, it is tempting to ascribe it to strong correlation effects, particularly since these effects are all either qualitatively in the direction expected for a correlated system or can conceivably arise from the additional complexity introduced by correlation effects.

On the other hand, chemical trends lead to the expectation that, all things being equal, 4d Ru oxides should be less prone to strongly correlated behavior than the corresponding 3d oxides, and much less prone to such effects than cuprates. This is because of the much more extended 4d orbitals in Ru ions which should lead to stronger hybridization, better screening, and lower effective Hubbard U . Furthermore, although much of the data are at first sight qualitatively in accordance with general expectations for a correlated system, they have not been quantitatively explained in these terms, and there are some data that are rather difficult to understand purely in terms of a correlated scenario, most notably the disappearance of magnetism upon doping Ca in the SrRuO₃ system and the ferromagnetic ground state in the integer occupancy (and thus not a double-exchange system) compound SrRuO₃.

We have performed first principles, band-structure-based calculations within the LSDA for SrRuO₃, CaRuO₃, and Sr₂YRuO₆. Although this approach fails miserably in systems that are truly strongly correlated, it does yield the correct magnetic and electronic states in these materials, including quantitative agreement with known magnetic properties in all cases in these ruthenates. Moreover, the different magnetic behaviors can be fully understood in terms of simple

and straightforward one-electron tight-binding models and Stoner theory. Although interpretation of the transport properties in terms of a conventional one-electron picture and Bloch-Boltzmann theory is not as straightforward, we show that such an approach is not inconsistent with the existing body of experimental evidence. A key notion for understanding the transport in these systems is strong electron-phonon-(para)magnon coupling, which in turn can be understood in the framework of the band theory.

In agreement with expectations based on chemical trends, rather strong hybridization is found between the Ru $4d$ and O $2p$ states in these materials. While antagonistic to a strong correlation scenario this is in large part responsible for the unusual properties in our band picture, including the very fact that magnetism occurs at all in a $4d$ metallic oxide. This strong hybridization leads to a ferromagnetic direct exchange interaction between Ru and O, and the cooperation between Ru and O contributions to the Stoner parameter leads to the magnetic ground states. As a result, the O ions in these ruthenates make substantial contributions to the magnetization density, which may be observable in neutron scattering experiments with O form factors included in the refinements. The importance of p - d hybridization also leads to a strong coupling of magnetic and structural degrees of freedom, resulting in, for example, the destabilization of the ferromagnetic state due to octahedral tilting in CaRuO_3 .

One consequence of our scenario is that when Ru ions are bonded to the same O, as neighboring Ru ions are in the perovskite structure, the interaction between them will be strongly ferromagnetic. This means that magnetic fluctuations in layered ruthenates like Sr_2RuO_4 and the associated Ruddlesden-Popper (RP) series of compounds are predicted to have predominantly ferromagnetic character in plane, although alternating layers or perovskite blocks in the RP series may be coupled antiferromagnetically to each other via superexchange through rocksalt blocks. Such ferromagnetic fluctuations would be pair breaking for singlet (s - or d -wave) superconductivity, but not for triplet superconductivity, as suggested for instance by Rice and Sigrist²⁶ for Sr_2RuO_4 . In fact, for triplet pairing both magnetic fluctuations and phonons provide Cooper attraction. Finally, when Ru ions are not connected at all via common O ions, like in Sr_2YRuO_6 the Ru-Ru coupling is via two intervening O ions, both of which are strongly hybridized with and ferromagnetically coupled to the nearest Ru, but couple to each other via an antiferromagnetic superexchange interaction. This results in an antiferromagnetic state.

The strength and importance of covalent transition-metal-oxygen interactions, combined with magnetism and metallicity, are perhaps unique to these ruthenates. Already a number of interesting physical properties have been found among these compounds, and no doubt more interesting physics remains to be found in this family.

ACKNOWLEDGMENTS

We acknowledge enlightening discussions with J.S. Dodge, R.P. Guertin, Lior Klein, Mark Lee, and W.E. Pickett. Work at the Naval Research Laboratory is supported by the Office of Naval Research. Computations were performed

using the DOD HPCMO computing centers at NAVO and ASC.

APPENDIX

Introduced by Fert and Campbell⁴⁹ and often used since then, the two-current conduction model of transport in ferromagnetic metals assumes that the spin-up and spin-down distribution function changes are independent. This formula was derived for a very specific case of s - d scattering in transition metals and under a number of simplifying assumptions. In the original papers⁴⁹ no clear distinction was made between the spin-flip scattering (which always influences the total conductivity) and the spin-flip conductivity (which vanishes when scattering-in is neglected). In a later publication⁵⁵ this distinction has been made, but this publication is less well known. We find it instructive to present here a systematic derivation for the two-current model of electric transport in ferromagnets and to show how it is related to the general theory of multiband conductivity. This derivation is based on Allen's variational approach to multiband Boltzmann equation^{56,47} and clearly shows some limits to the applicability of the two-current model.

The Boltzmann equation for electric transport in metals is

$$\begin{aligned} e\mathbf{E}\cdot\mathbf{v}_{i\mathbf{k}}\frac{\partial f}{\partial\epsilon_{i\mathbf{k}}} &= \sum_{j\mathbf{k}'} P_{i\mathbf{k},j\mathbf{k}'}(\delta f_{i\mathbf{k}} - \delta f_{j\mathbf{k}'}) \\ &= \delta f_{i\mathbf{k}}\sum_{j\mathbf{k}'} P_{i\mathbf{k},j\mathbf{k}'} - \sum_{j\mathbf{k}'} P_{i\mathbf{k},j\mathbf{k}'}\delta f_{j\mathbf{k}'}, \end{aligned}$$

where the subscripts i, j include both the band index and the spin and P is the transition probability matrix element, which can also be written conveniently in terms of the scattering matrix elements M as

$$P_{i\mathbf{k},j\mathbf{k}'} = M_{i\mathbf{k},j\mathbf{k}'}^2 \delta(\epsilon_{i\mathbf{k}} - \epsilon_{j\mathbf{k}'})$$

for static (impurity) scattering, or the corresponding expression for the scattering by phonons, magnons etc. The change of the distribution function for given \mathbf{k} is $\delta f_{i\mathbf{k}} = -\phi_{i\mathbf{k}}(\partial f/\partial\epsilon_{i\mathbf{k}})$, so that

$$e\mathbf{E}\cdot\mathbf{v}_{i\mathbf{k}}\frac{\partial f}{\partial\epsilon_{i\mathbf{k}}} = \sum_{j\mathbf{k}'} P_{i\mathbf{k},j\mathbf{k}'} \left(\frac{\partial f}{\partial\epsilon_{i\mathbf{k}}} \phi_{i\mathbf{k}} - \frac{\partial f}{\partial\epsilon_{j\mathbf{k}'}} \phi_{j\mathbf{k}'} \right)$$

and for $T \rightarrow 0$

$$\begin{aligned} e\mathbf{E}\cdot\mathbf{v}_{i\mathbf{k}}\delta(\epsilon_{i\mathbf{k}} - E_F) &= \sum_{j\mathbf{k}'} M_{i\mathbf{k},j\mathbf{k}'}^2 (\phi_{i\mathbf{k}} - \phi_{j\mathbf{k}'}) \delta(\epsilon_{i\mathbf{k}} - \epsilon_{j\mathbf{k}'}) \delta(\epsilon_{i\mathbf{k}} - E_F) \\ &= \sum_{j\mathbf{k}'} M_{i\mathbf{k},j\mathbf{k}'}^2 (\phi_{i\mathbf{k}} - \phi_{j\mathbf{k}'}) \delta(\epsilon_{j\mathbf{k}'} - E_F) \delta(\epsilon_{i\mathbf{k}} - E_F). \end{aligned}$$

Allen introduced (and called ‘‘disjoint representation’’) the following approximation: For each sheet of the Fermi surface $\phi_{i\mathbf{k}}$ is proportional to $\mathbf{v}_{i\mathbf{k}}$, $\phi_{i\mathbf{k}} = a_i \mathbf{v}_{i\mathbf{k}} \cdot e\mathbf{E}$, where the coefficients a depend on the band (and, in a magnet, on the spin). In this approximation, the last equation may be solved (we assume $\mathbf{E} \parallel x$ and omit subscript x at v):

$$\sum_{\mathbf{ik}} v_{\mathbf{ik}}^2 \delta(\epsilon_{\mathbf{ik}} - E_F) = \sum_{\mathbf{ik}, \mathbf{jk}'} M_{\mathbf{ik}, \mathbf{jk}'}^2 (a_i v_{\mathbf{ik}}^2 - a_j \mathbf{v}_{\mathbf{ik}} \cdot \mathbf{v}_{\mathbf{jk}'}) \times \delta(\epsilon_{\mathbf{jk}'} - E_F) \delta(\epsilon_{\mathbf{ik}} - E_F)$$

or

$$\langle Nv^2 \rangle_i = \sum_j Q_{ij} a_j,$$

where the shorthand notation on the left-hand side is obvious and

$$\begin{aligned} Q_{ij} &= \delta_{ij} \sum_j \sum_{\mathbf{kk}'} M_{\mathbf{ik}, \mathbf{jk}'}^2 v_{\mathbf{ik}}^2 \delta(\epsilon_{\mathbf{ik}} - E_F) \delta(\epsilon_{\mathbf{jk}'} - E_F) \\ &\quad - \sum_{\mathbf{kk}'} M_{\mathbf{ik}, \mathbf{jk}'}^2 \mathbf{v}_{\mathbf{ik}} \cdot \mathbf{v}_{\mathbf{jk}'} \delta(\epsilon_{\mathbf{ik}} - E_F) \delta(\epsilon_{\mathbf{jk}'} - E_F) \\ &= \delta_{ij} \sum_j \langle NM^2 Nv^2 \rangle_{ij} - \langle NvM^2 Nv \rangle_{ij}. \end{aligned}$$

The first term here accounts for the scattering-out and the second for the scattering-in processes. Solving now for a 's, we find

$$a_i = \sum_j Q_{ij}^{-1} \langle Nv^2 \rangle_j,$$

since the total current density is

$$\begin{aligned} \mathbf{j} &= -2e \sum_{\mathbf{ik}} \mathbf{v}_{\mathbf{ik}} \phi_{\mathbf{ik}} \delta(\epsilon_{\mathbf{ik}} - E_F) \\ &= -2e^2 \sum_{\mathbf{ik}} v_{\mathbf{ik}}^2 \delta(\epsilon_{\mathbf{ik}} - E_F) a_i \mathbf{E} = -2e^2 \sum_j \langle Nv^2 \rangle_j a_j \mathbf{E} \end{aligned}$$

and the conductivity is

$$\sigma = e^2 \sum_{ij} \langle Nv^2 \rangle_i Q_{ij}^{-1} \langle Nv^2 \rangle_j.$$

In notation of Fert and Campbell^{49,55} this is

$$\sigma = \sum_{ss'} \rho_{ss'}^{-1},$$

analogous to Eq. (57) of Ref. 47. The Campbell-Fert formula is different when the nondiagonal elements are not neglected. It gives instead

$$\sigma = (\rho_1 + \rho_2 + 4\rho_{12}) / (\rho_1 \rho_2 + \rho_1 \rho_{12} + \rho_2 \rho_{12}).$$

For the purpose of this paper we shall neglect scattering-in completely, because it is defined by an average over the sign-changing quantity $\mathbf{v}_{\mathbf{ik}} \cdot \mathbf{v}_{\mathbf{jk}'}$, so that the matrix Q is diagonal. We shall also define the partial resistivities differently from Refs. 49 and 55, namely, so that

$$\rho_{ij} = \langle Nv^2 M^2 \rangle_{ij} / 2e^2 \langle Nv^2 \rangle_i^2 = \frac{1}{e^2 \tau_{ij}} \left/ \left(\frac{n}{m} \right)_i^{\text{eff}} \right.$$

So defined, the $\rho_{\uparrow\downarrow}$ is proportional to the spin-flip scattering rate. Then, for a simple ferromagnet with the two Fermi surface sheets, one for spin-up and another for spin-down electrons, we have

$$\sigma = (\rho_{\uparrow} + \rho_{\uparrow\downarrow})^{-1} + (\rho_{\downarrow} + \rho_{\uparrow\downarrow})^{-1}$$

or

$$\rho = (\rho_{\uparrow} \rho_{\downarrow} + \rho_{\downarrow} \rho_{\uparrow\downarrow} + \rho_{\uparrow} \rho_{\downarrow\uparrow} + \rho_{\uparrow\downarrow} \rho_{\downarrow\uparrow}) / (\rho_{\uparrow} + \rho_{\downarrow} + \rho_{\uparrow\downarrow} + \rho_{\downarrow\uparrow}).$$

This coincides with the Fert-Campbell formula if the scattering-in term is neglected; otherwise, it is different.

-
- ¹C.B. Eom, R.J. Cava, R.M. Fleming, J.M. Phillips, R.B. van Dover, J.H. Marshall, J.W.P. Hsu, J. J. Krajewski, and W.F. Peck, Jr., *Science* **258**, 1766 (1992).
- ²D. Kirillov, Y. Suzuki, L. Antognazza, K. Char, I. Bozovic, and T.H. Geballe, *Phys. Rev. B* **51**, 12 825 (1995).
- ³M. Shikano, T.K. Huang, Y. Inaguma, M. Itoh, and T. Nakamura, *Solid State Commun.* **90**, 115 (1994).
- ⁴M. Itoh, M. Shikano, and T. Shimura, *Phys. Rev. B* **51**, 16 432 (1995).
- ⁵L. Klein, J.S. Dodge, T.H. Geballe, A. Kapitulnik, A.F. Marshall, L. Antognazza, and K. Char, *Appl. Phys. Lett.* **66**, 2427 (1995).
- ⁶D.J. Singh, *J. Appl. Phys.* **79**, 4818 (1996).
- ⁷J.J. Neumeier, A.L. Cornelius, and J.S. Schilling, *Physica B* **198**, 324 (1994).
- ⁸S.A. Carter, B. Batlogg, R.J. Cava, J.J. Krajewski, W.F. Peck, Jr., and L.W. Rupp, Jr., *Phys. Rev. B* **51**, 17 184 (1995).
- ⁹J.S. Gardner, G. Balakrishnan, and D.M.K. Paul, *Physica C* **252**, 303 (1995).
- ¹⁰A. Gulino, R.G. Egdell, P.D. Battle, and S.H. Kim, *Phys. Rev. B* **51**, 6827 (1995).
- ¹¹S.C. Gausepohl, M. Lee, K. Char, R.A. Rao, and C.B. Eom, *Phys. Rev. B* **52**, 3459 (1995).
- ¹²S.C. Gausepohl, M. Lee, R.A. Rao, and C.B. Eom, *Phys. Rev. B* **54**, 8996 (1996).
- ¹³G. Cao, S. McCall, J. Bolivar, M. Shepard, F. Freibert, P. Henning, J.E. Crow, and T. Yuen, *Phys. Rev. B* **54**, 15 144 (1996).
- ¹⁴J.H. Cho, Q.X. Jia, X.D. Wu, S.R. Foltyn, and M.P. Maley, *Phys. Rev. B* **54**, 37 (1996).
- ¹⁵L. Klein, J.S. Dodge, C.H. Ahn, G.J. Snyder, T.H. Geballe, M.R. Beasley, and A. Kapitulnik, *Phys. Rev. Lett.* **77**, 2774 (1996).
- ¹⁶Y. Maeno, H. Hashimoto, K. Yoshida, S. Nishizaki, T. Fujita, J.G. Bednorz, and F. Lichtenberg, *Nature (London)* **372**, 532 (1994).
- ¹⁷T. Oguchi, *Phys. Rev. B* **51**, 1385 (1995).
- ¹⁸D.J. Singh, *Phys. Rev. B* **52**, 1358 (1995).
- ¹⁹T. Vogt and D.J. Buttrey, *Phys. Rev. B* **52**, R9843 (1995).
- ²⁰N. Shirakawa, K. Murata, Y. Nishihara, S. Nishizaki, Y. Maeno, T. Fujita, J.G. Bednorz, F. Lichtenberg, and N. Hamada, *J. Neurophysiol.* **64**, 1072 (1995).
- ²¹M. Schmidt, T.R. Cummins, M. Burk, D.H. Lu, N. Nucker, S. Schuppler, and F. Lichtenberg, *Phys. Rev. B* **53**, R14 761 (1996).
- ²²A.P. Mackenzie, S.R. Julian, A.J. Diver, G.J. McMullan, M.P. Ray, G.G. Lonzarich, Y. Maeno, S. Nishizaki, and T. Fujita,

- Phys. Rev. Lett. **76**, 3786 (1996).
- ²³T. Yokoya, A. Chainani, T. Takahashi, H. Katayama-Yoshida, M. Kasai, Y. Tokura, N. Shanthi, and D.D. Sarma, Phys. Rev. B **53**, 8151 (1996).
- ²⁴T. Yokoya, A. Chainani, T. Takahashi, H. Katayama-Yoshida, M. Kasai, and Y. Tokura, Phys. Rev. Lett. **26**, 3009 (1996).
- ²⁵D.H. Lu, M. Schmidt, T.R. Cummins, S. Schuppler, F. Lichtenberg, and J.G. Bednorz, Phys. Rev. Lett. **76**, 4845 (1996).
- ²⁶T.M. Rice and M. Sigrist, J. Phys. Condens. Matter **7**, L643 (1995).
- ²⁷P.B. Allen, H. Berger, O. Chauvet, L. Forro, T. Jarlborg, A. Junod, B. Revaz, and G. Santi, Phys. Rev. B **5**, 4393 (1996).
- ²⁸T. Kiyama, K. Yoshimura, K. Kosuge, Y. Ikeda, and Y. Bando, Phys. Rev. B **54**, R756 (1996).
- ²⁹J.J. Randall and R. Ward, J. Am. Chem. Soc. **81**, 2629 (1959).
- ³⁰A. Callaghan, C.W. Moeller, and R. Ward, Inorg. Chem. **5**, 1572 (1966).
- ³¹J.M. Longo, P.M. Raccah, and J.B. Goodebough, J. Appl. Phys. **39**, 1327 (1968).
- ³²C.W. Jones, P.D. Battle, P. Lightfoot, and W.T.A. Harrison, Acta Crystallogr. Sec. C **45**, 365 (1989).
- ³³A. Kanbayashi, J. Phys. Soc. Jpn. **44**, 108 (1978).
- ³⁴M.K. Wu, D.Y. Chen, F.Z. Chien, S.R. Sheen, D.C. Ling, C.Y. Tai, G.Y. Tseng, D.H. Chen, and F.C. Zhang, Z. Phys. B **102**, 37 (1997).
- ³⁵J.J. Neumeier, M.F. Hundley, M.G. Smith, J.D. Thompson, C. Allgeier, H. Xie, W. Yelon, and J.S. Kim, Phys. Rev. B **50**, 17 910 (1994).
- ³⁶G. Baskaran, Physica B **233&224**, 490 (1996).
- ³⁷J.E. Crow (unpublished).
- ³⁸P.D. Battle and W.J. Maclin, J. Solid State Chem. **54**, 245 (1984).
- ³⁹D.J. Singh, *Planewaves Pseudopotentials and the LAPW method* (Kluwer, Boston, 1994), and references therein.
- ⁴⁰D. Singh, Phys. Rev. B **43**, 6388 (1991).
- ⁴¹O.K. Andersen, Phys. Rev. B **12**, 3060 (1975); O.K. Andersen and O. Jepsen, Phys. Rev. Lett. **53**, 2571 (1984).
- ⁴²R. Liebmann, *Statistical Mechanics of Periodic Frustrated Ising Systems* (Springer, Berlin, 1986).
- ⁴³N.D. Mackenzie and A.P. Young, J. Phys. C **14**, 3227 (1981).
- ⁴⁴J.C. Slater, Phys. Rev. **49**, 537 (1936); E.C. Stoner, Proc. R. Soc. London, Ser. A **165**, 372 (1938).
- ⁴⁵G. L. Krasko, Phys. Rev. B **36**, 8565 (1987); O.K. Andersen *et al.*, Physica B&C **86-88**, 249 (1977).
- ⁴⁶Note that we have not optimized the structure either for the paramagnetic or for the magnetic structures in our fixed-moment calculations. Due to strong magnetoelastic interactions, the equilibrium tilting angle in a magnetic state should be slightly different from that without magnetization. However, the qualitative statement that CaRuO₃ is on the verge of magnetic instability should be true even if magnetoelastic effects are taken into account.
- ⁴⁷F.J. Pinski, P.B. Allen, and W. Butler, Phys. Rev. B **23**, 5080 (1981).
- ⁴⁸I.I. Mazin, A.I. Liechtenstein, C.O. Rodriguez, O. Jepsen, and O.K. Andersen, Physica C **209**, 125 (1993).
- ⁴⁹A. Fert and I.A. Campbell, Phys. Rev. Lett. **21**, 1190 (1968); A. Fert, J. Phys. C **2**, 1784 (1969).
- ⁵⁰R.J. Bouchard and J.L. Gillson, Mater. Res. Bull. **7**, 873 (1972).
- ⁵¹D.L. Mills, A. Fert, and I.A. Campbell, Phys. Rev. B **4**, 196 (1971).
- ⁵²A. I. Schindler and M.J. Rice, Phys. Rev. **164**, 759 (1967).
- ⁵³W.W. Schulz, P.B. Allen, and N. Trivedi, Phys. Rev. B **45**, 10 886 (1992).
- ⁵⁴R.P. Guertin (private communication).
- ⁵⁵I.A. Campbell and A. Fert, in *Ferromagnetic Materials*, edited by E.P. Wolfarth (North-Holland, Amsterdam, 1982), Vol. 3, p. 747.
- ⁵⁶P.B. Allen, Phys. Rev. B **17**, 3725 (1978).